

# Deep invariant networks with differentiable augmentation layers

Cédric Rommel, Thomas Moreau & Alexandre Gramfort  
Université Paris-Saclay, Inria, CEA, Palaiseau, 91120, France  
{firstname.lastname}@inria.fr

arXiv:2202.02142v3 [cs.LG] 16 Feb 2022

## Abstract

Designing learning systems which are invariant to certain data transformations is critical in machine learning. Practitioners can typically enforce a desired invariance on the trained model through the choice of a network architecture, e.g. using convolutions for translations, or using data augmentation. Yet, enforcing true invariance in the network can be difficult, and data invariances are not always known *a priori*. State-of-the-art methods for learning data augmentation policies require held-out data and are based on bilevel optimization problems, which are complex to solve and often computationally demanding. In this work we investigate new ways of learning invariances only from the training data. Using learnable augmentation layers built directly in the network, we demonstrate that our method is very versatile. It can incorporate any type of differentiable augmentation and be applied to a broad class of learning problems beyond computer vision. We provide empirical evidence showing that our approach is easier and faster to train than modern automatic data augmentation techniques based on bilevel optimization, while achieving comparable results. Experiments show that while the invariances transferred to a model through automatic data augmentation are limited by the model expressivity, the invariance yielded by our approach is insensitive to it by design.

## 1 Introduction

Inductive biases encoding known data symmetries are key to make deep learning models generalize in high-dimensional settings such as computer vision, speech processing and computational neuroscience, just to name a few. Convolutional layers [LeCun et al. \[1989\]](#) are the

perfect illustration of this, as their translation equivariant property allowed to reduce dramatically the size of the hypothesis space compared to fully-connected layers, opening the way for modern computer vision achievements [Krizhevsky et al. \[2012\]](#). This illustrates one way to encode desired symmetries in deep learning models by hard-coding them directly in the network architecture. An alternative way is to use data augmentation, where transformations encoding the desired symmetries are applied to the training examples, thus adding additional cost when such symmetry is not recognized by the model. While in the first case invariances are *built in* the network by design and are therefore a hard constraint, data augmentation promotes certain invariances more softly. As opposed to being *built-in*, desired invariances are here *trained-in* [Zhou et al. \[2021\]](#).

In both cases, the invariances present in the data are not always known beforehand. While relevant invariances are intuitive for some tasks such as object recognition (e.g. a slightly tilted or horizontally flipped picture of a mug, still represents a mug), the same cannot be said for many important predictive tasks such as classifying brain signals into different sleep stages [Chambon et al. \[2018\]](#), [Phan et al. \[2021\]](#). In order to be able to tackle this problem of learning optimal systems from complex data two strategies are pursued in the literature: neural architecture search (NAS) which aims to find the best architectural elements from the training data, and automatic data augmentation (ADA) which aims to learn augmentation policies automatically from a given dataset. Both fields tackle the problem very similarly, by parametrizing the network architecture or the augmentation policies, leading to a bilevel hyperparameters optimization problem [Cubuk et al. \[2019\]](#). While these techniques allowed to find architectures and augmentations capable of outperforming the state-of-the-art in some cases, solving such bilevel optimization problems is often difficult and computationally demanding [Zela et al. \[2019\]](#), [Chen & Hsieh \[2020\]](#), [Zhang et al. \[2021\]](#).

This work investigates how to learn data invariances

---

Do not distribute. Copyright 2022 by the authors.

directly from the training data, avoiding the complex bilevel structure of ADA. To this end, we propose to integrate learnable data augmentation layers within the network, and train them together with other model parameters using a novel invariance promoting regularizer. Our approach extends previous works into a very general framework that goes beyond computer vision tasks, as it can incorporate any type of differentiable augmentations. We demonstrate the *versatility* of our method on two well controlled simulated settings, as well as an image recognition and a sleep stage classification dataset. We show that our approach can correctly select the transformations to which the data is invariant, and learn the true range of invariance, even for nonlinear operations. Our experiments also demonstrate that the data augmentation layer proposed here leads to almost perfect built-in invariances irrespective to the complexity of the original network it is added to. Moreover, we are able to achieve comparable performance and speed as state-of-the-art ADA approaches on our sleep staging experiment with a completely *end-to-end* approach, avoiding tedious bilevel optimization parameters.

## 2 Related work

**Automatic data augmentation** Automatic data augmentation aims to learn relevant data invariances which increase generalization power. More precisely, ADA is about searching augmentations that, when applied during the model training, will minimize its validation loss. This objective is summarized in the following bilevel optimization problem:

$$\begin{aligned} \min_{\mathcal{T}} \quad & \mathcal{L}(\theta^* | D_{\text{valid}}) \\ \text{s.t.} \quad & \theta^* \in \arg \min_{\theta} \mathcal{L}(\theta | \mathcal{T}(D_{\text{train}})) , \end{aligned} \quad (1)$$

where  $\mathcal{T}$  is an augmentation policy,  $\theta$  denotes the parameters of some predictive model, and  $\mathcal{L}(\theta|D)$  its loss over the set  $D$ . Initial ADA approaches such as AutoAugment Cubuk et al. [2019] and PBA Ho et al. [2019] use discrete search algorithms to approximately solve (1). Despite the impressive results obtained, they are tremendously costly in computation time, which makes them impractical in many realistic settings. In an attempt to alleviate this limitation, Fast AutoAugment Lim et al. [2019] proposes to solve a surrogate density matching problem, which breaks the bilevel structure of (1). It is hence substantially faster to solve, since it does not require to train the model multiple times. However, this method needs a pre-trained model and its success highly depend on whether the latter was able to learn relevant data invariances on its own. Another way of carrying ADA efficiently is by using gradient-based algorithms, as proposed in Faster AutoAugment Hataya

et al. [2020], DADA Li et al. [2020] and ADDA Rommel et al. [2021]. While Faster AutoAugment also tackles a surrogate density matching problem, DADA and ADDA solve the bilevel problem (1) directly. These ADA methods are the most related to our work since we rely on the same differentiable relaxations of standard augmentation transformations. However, we are mostly interested in building the learned invariances into the model, which is out of the scope of these methods. Indeed, they require substantially more overhead than our approach since they learn augmentations from the validation set and need to retrain the model after the augmentation search is completed. Moreover, DADA and ADDA are based on an alternating optimization of the inner and outer problems Liu et al. [2019], which suffer from noisy hypergradients on the outer level due to the stochastic inner problem, and require careful tuning of the outer learning rate Zela et al. [2019], Chen & Hsieh [2020], Zhang et al. [2021].

### Embedding invariances within neural network architecture

A vast literature has focused on encoding predefined invariances or equivariances into neural network architectures. For instance, group convolutions allow to extend traditional convolutional layers to groups of affine transformations other than translations Cohen & Welling [2016]. More related to our work, DeepSets Zaheer et al. [2017] encode permutation invariance by summing networks predictions. Although related, these methods are not designed for learning symmetries from the data, which is the objective of this study.

Prior work on this matter from van der Wilk et al. [2018] proposes to learn invariances using the marginal likelihood in the context of Gaussian processes. In contrast, we are mostly focused on deep neural networks. Zhou et al. [2021] suggests to discover data symmetries and build them into neural networks by learning weight sharing patterns in a meta-learning framework. Most related to our work is Augerino Benton et al. [2020], which allows to learn invariances to affine transformations from the training data, by adding a learnable sampling brick to an existing model and averaging its predictions. They propose to learn the range of distributions from which affine transformations are sampled, by parametrizing the corresponding Lie group in terms of its Lie algebra. As it is unclear how to extend Augerino beyond Lie groups such as affine transformations, its scope of application is rather limited, making it mostly tailored for computer vision tasks. In this work we build on their ideas, extending Augerino to more diverse applications with hierarchical differentiable data augmentation layers built into the networks. Moreover, in addition to learning sampling distribution ranges, we also learn to

select transformations which encode the strongest data invariance.

### 3 AugNet: A general framework to embed data augmentation into neural networks

#### 3.1 Preliminaries

Let us consider a dataset  $(x_1, y_1), \dots, (x_N, y_N)$  of observations sampled from an unknown distribution  $\mathbb{P}_{X,Y}$  over  $\mathcal{X} \times \mathcal{Y}$ . In a supervised setting, one wants to use this data to train a model  $f : \mathcal{X} \rightarrow \mathcal{Y}$  (e.g. a neural network) so that it can predict  $y$  from new observations  $x$  sampled from the marginal  $\mathbb{P}_X$ . Now, suppose that the data joint distribution  $\mathbb{P}_{X,Y}$  is invariant to a certain group  $G$  of transformations acting on  $\mathcal{X}$ , i.e. for any  $g \in G$  the distribution  $\mathbb{P}_{X,Y}$  is close (in some sense) to the transformed distribution  $\mathbb{P}_{gX,Y}$  (cf. [Chen et al. \[2020\]](#) for further details). This means for example that, if  $Y = y$  is the class "dog", then the probability of sampling an image  $X = x$  of a dog is close to the probability of sampling the transformed image  $gx$ . In this situation, one would like the model  $f$  to have this same invariance by design, so that it does not have to learn it from scratch and can better generalize to new observations of  $\mathbb{P}_{X,Y}$ . In other words, we would like  $f(gx) = f(x)$  for any  $g \in G$ . One way of achieving this is to average  $f$  over  $G$  endowed with a uniform distribution  $\nu_G$ :

**Proposition 3.1.** *For a given model  $f : \mathcal{X} \rightarrow \mathcal{Y}$  and a group of transformations  $G$  acting on  $\mathcal{X}$ ,  $\bar{f} : \mathcal{X} \rightarrow \mathcal{Y}$  defined as*

$$\bar{f}(x) = \mathbb{E}_{g \sim \nu_G} [f(gx)] \ ,$$

where  $\nu_G$  is a uniform distribution on  $G$ , is invariant through the action of  $G$ .

The proof follows from the assumption that  $\nu_G$  is uniform and  $G$  is a group, hence stable by composition and inverse. So for any  $u \in G$ ,  $gu^{-1}$  is also in  $G$  and

$$\begin{aligned} \bar{f}(ux) &= \mathbb{E}_{g \sim \nu_G} [f(gux)] = \mathbb{E}_{hu^{-1} \sim \nu_G} [f(hx)] \\ &= \mathbb{E}_{h \sim \nu_G} [f(hx)] = \bar{f}(x) \ , \end{aligned}$$

where  $h = gu$ . In practice, we will consider sets of transformations  $G$  which do not necessarily form a group (e.g. rotations within a given range). Because of this,  $\bar{f}$  is only approximately invariant, although it can get very close to perfect invariance, as shown in our experiments from [Section 4.3](#).

#### 3.2 Architecture: augment, forward and aggregate

As the averaged model (3.1) is intractable, one can approximate it with an empirical average

$$\tilde{f}(x) = \frac{1}{C} \sum_{c=1}^C f(g_c x),$$

where  $g_c$ 's are sampled from  $\nu_G$ . In practice, using a large number  $C$  of sampled transformations would be prohibitive as well. Fortunately, even when  $C$  is small,  $\tilde{f}$  is an unbiased estimator of  $\bar{f}$ . Hence stochastic gradient descent can be used to train *exactly*  $\bar{f}$  by minimizing the loss of  $\tilde{f}$ .

Based on these observations, we propose to create nearly invariant neural networks made of three blocks:

- an *augmentation module*, which takes an input  $x \in \mathcal{X}$ , samples  $C$  transformations from  $G$ , and outputs  $C$  transformed copies of  $x$ ;
- a *trunk model*  $f$ , which can be any neural network mapping transformed inputs to predictions;
- and an *aggregation module*, which is responsible for averaging the  $C$  predictions.

This general architecture is illustrated on [Figure 1](#) and referred to as *AugNet* hereafter. Note that unlike standard data augmentation, the transformations distributions is part of the model and kept at inference.

#### 3.3 Augmentation layers

There are two missing elements from the architecture described in the previous section, namely the choice of the set of transformations  $G$  and how transformations are sampled from it. Indeed, the true invariances present in a dataset are often unknown, which is why we propose to learn both the set of transformations and a parametrized distribution used to sample from them.

In this paper, we are mostly interested in transformations  $T : \mathcal{X} \rightarrow \mathcal{X}$  defining a data augmentation, such as random rotations in image recognition. Most often, such operations can transform the data with more or less intensity depending on a parameter  $\mu$ , called *magnitude* hereafter. If we take the same example of random rotations, the magnitude can be the maximum angle by which we are allowed to rotate the images. In order to have an homogeneous scale for all transformations considered, we assume without loss of generality that magnitudes lie in the interval  $[0, 1]$ , with  $\mu = 0$  being equivalent to the identity (i.e. no augmentation) and  $\mu = 1$  being the maximal transformation strength considered. By using the reparametrization trick [Schulman](#)

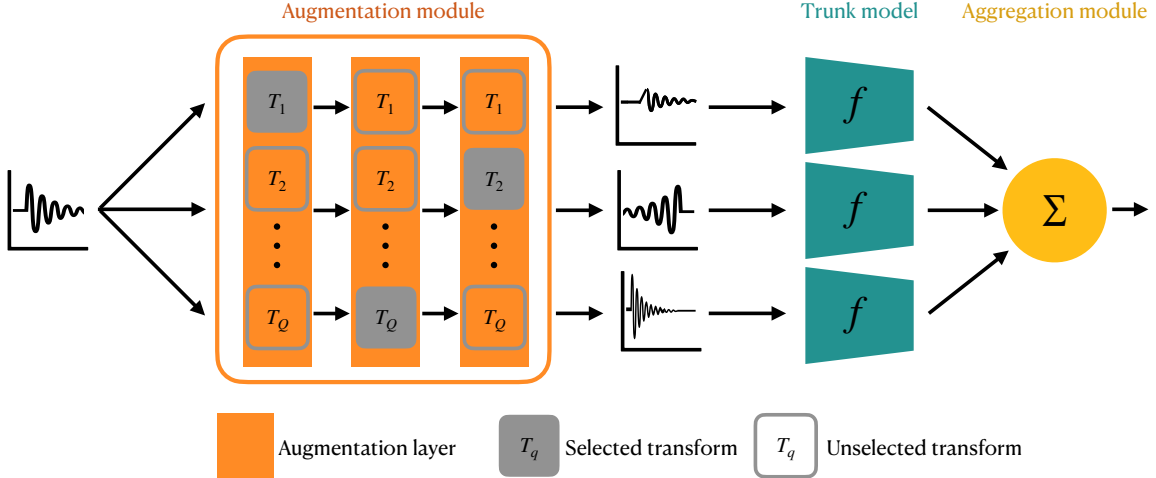


Figure 1: General architecture of AugNet. Input data is copied  $C$  times and randomly augmented by the augmentation layers forming the *augmentation module*. Each copy is then mapped by the *trunk model*  $f$ , whose predictions are averaged by the *aggregation module*. Parameters of both  $f$  and the augmentation layers are learned together from the training set.

et al. [2015] or some other type of gradient estimator such as straight-through Bengio et al. [2013] or relax Grathwohl et al. [2018], these transformations can be made differentiable with respect to  $\mu$  as shown for example by Hataya et al. [2020] for image augmentations and by Rommel et al. [2021] for augmentations of electroencephalography signals (EEG). One can hence learn the right magnitude to use from the data by backpropagating gradients through  $T$ .

But the correct transformation  $T$  describing a data invariance is also supposed to be unknown and needs to be learned in addition to its magnitude. Let  $\mathcal{T} = \{T_1, \dots, T_Q\}$  be a discrete set of transformations possibly describing a data invariance. We propose to use backpropagation to learn which transformation to pick from this set by using a layer consisting of a weighted average of all transformations:

$$\text{AugLayer}(x; w, \mu) = \sum_{q=1}^Q w_q T_q(x; \mu_q), \quad (2)$$

where the weights  $w_q$  sum to 1. In practice, we optimize some other hidden weights  $w'$  which pass through a softmax activation  $w = \sigma(w')$ . As explained in Section 3.4 and demonstrated in our experiments, this layer architecture favors a single transformation describing a correct data invariance and tune its magnitude.

As the data might be invariant to more than one transformation, these layers can be stacked on top of each other, so that each one learns a different transformation (see Figure 1). This is justified by the stability property of invariance for composition. Indeed,

if a function  $h : \mathcal{X} \rightarrow \mathcal{Y}$  is invariant to actions  $u$  and  $g$ , then it must be invariant to their composition:  $h((u \circ g)x) = h(u(gx)) = h(gx) = h(x)$ . Hence, we build augmentation modules with sequences of augmentation layers (2) and learn their parameters  $w, \mu$  from the training set together with the parameters of the trunk model.

### 3.4 Selective regularizer

As illustrated in our experiments from Section 4.1, if we train *AugNet* with a standard loss such as the cross-entropy, the model tends to find the most unconstrained model: the one with  $\mu = 0$ , which never augments the data. The same was described for Augerino Benton et al. [2020], which is why its authors proposed to add a regularization  $R$  pushing towards broader distributions:

$$\min_{w, \mu, \theta} \ell(\tilde{f}(x; w, \mu, \theta), y) + \lambda R(\mu) . \quad (3)$$

In the previous equation,  $\theta$  denotes the parameters of the trunk neural network  $f$  and  $\ell$  is a loss function. With our formalism, the regularization proposed by Benton et al. [2020] is equivalent to penalizing the negative  $L_2$ -norm of the magnitude vector:  $R(\mu) = -\|\mu\|_2$ . As illustrated in the ablation experiments of Section 4.1, this regularizer is not sufficient to ensure that our augmentation layers do not converge to the identity transform because we have an additional degree of freedom than Augerino: the weights  $w$ . Hence, the model may reach low loss values by just maximizing the weight of a single transform  $w_q = 1$  with magnitude  $\mu_q = 0$ , while maximizing

all other magnitudes  $\mu_{q \neq q'} = 1$ . Because of this, we propose instead to penalize the norm of the element-wise product of weights and magnitudes:  $R(w, \mu) = -\|w \odot \mu\|_2$ . This has the effect of tying together  $w_q$  and  $\mu_q$  of the same transformation  $T_q$ , avoiding the problem described before.

Another property of this regularization is that it promotes the selection of a single transformation per augmentation layer, as illustrated on Figure 2 for the simple case of  $n = 2$  transformations. Because  $\sum_q w_q = w_1 + w_2 = 1$ , the vector  $w \odot \mu = (x_1, x_2) \in [0, 1]^2$  is bound to move within the line of equation  $x_2 = \mu_2(1 - \frac{x_1}{\mu_1})$  when the magnitudes  $\mu_1$  and  $\mu_2$  are fixed. At the beginning of the training, with all weights initialized at 0.5 and magnitudes close to 0, if neither  $T_1$  or  $T_2$  harm the training, the vector’s norm can grow following the bissector by increasing the magnitudes equally. Once one of the transformations  $T_1$  reaches a magnitude  $\bar{\mu}_1$ , it will start harming the training loss and its gradient will converge to 0. This introduces an imbalance between the transformations as  $\mu_2$  keeps increasing, until it reaches its maximal value  $\bar{\mu}_2 > \bar{\mu}_1$ . As  $w \odot \mu$  is still bound to move within the line  $\bar{\mu}_2(1 - \frac{x_1}{\bar{\mu}_1})$ , the only way to keep increasing its norm is by pointing more and more vertically, until it gets to  $w_2 = 1$  and  $w_1 = 0$ . This can also be seen from the expression of the gradients of the regularizer:

$$\frac{\partial R^2}{\partial w_i}(w, \bar{\mu}) = 2\bar{\mu}_i^2 - 2w_i(\bar{\mu}_1^2 + \bar{\mu}_2^2) .$$

which implies that:

$$\nabla_{w_1} R^2(w, \bar{\mu}) \leq \nabla_{w_2} R^2(w, \bar{\mu}) \iff \bar{\mu}_1 \leq \bar{\mu}_2 .$$

Each augmentation layer hence promotes the transformation with the highest admissible magnitude.

## 4 Experiments with synthetic data

In this section we present experimental results of *AugNet* in controlled settings in order to verify empirically some of its properties and compare it to *Augerino* and standard data augmentations.

### 4.1 Comparison to Augerino

**Learning the correct invariance** First, we reproduced the Mario-Iggy experiment by Benton et al. [2020] to show that AugNet can also learn affine invariances from image datasets. The data is generated from two initial images, which are rotated by a random angle either between  $[-\pi/4, \pi/4]$  (labels 0 and 2) or between  $[-\pi, -3\pi/4] \cup [3\pi/4, \pi]$  (labels 1 and 3). This procedure is illustrated in Figure A.1. Hence, labels depend

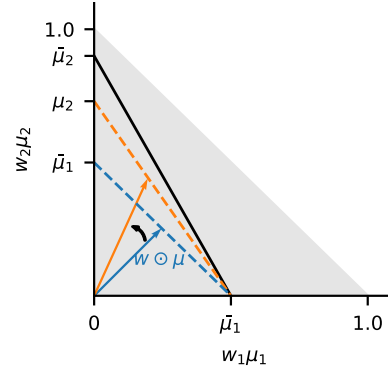


Figure 2: Illustration of the selective property of AugNet’s regularizer. As the norm of the vector  $w \odot \mu$  increases and  $\mu_1$  reaches the maximal value allowed by the training loss  $\bar{\mu}_1$ ,  $\mu_2$  starts getting greater than  $\mu_1$ , creating an imbalance in the weights gradients. When  $\mu_2$  reaches  $\bar{\mu}_2$ , the only way to keep increasing the vector’s norm is by decreasing  $w_1$  towards 0 and increasing  $w_2$  towards 1.

both on the initial image and on whether it has its head pointing up or down. By design, the data is invariant to inputs rotations between  $[-\pi/4, \pi/4]$ , and the experiments objective is to verify whether AugNet can learn this invariance. For this, we use a single augmentation layer containing 5 geometric augmentations: **translate-x**, **translate-y**, **rotate**, **shear-x** and **shear-y**. Note that while these augmentations are also encoded in Augerino, we don’t use the Lie algebra and exponential maps to implement them here. Maximal translations are set to half the image width/height, maximal rotations correspond to an angle of  $\pm\pi$  and maximal shearing coefficients are 0.3. The trunk model used is a simple 5-layer convolutional network, whose architecture is described in Section A.1 together with other experimental details. As shown on Figure 3, both Augerino (blue) and AugNet (orange) are capable of learning the correct angle of invariance from the data.

**Ablation study** As explained in Section 3.4, the regularizer plays a crucial role both in AugNet and Augerino. It can be seen on Figure 3 that without regularization the rotation angle converges to 0. Indeed, our model naturally tends to nullify any transformations of the input, similarly to what is shown by Benton et al. [2020] for Augerino. Furthermore, we also see that when we replace AugNet’s regularizer by Augerino’s one ( $-\|\mu\|_2$ ), the model does not learn the correct angle. This happens because this penalty is not sufficient to prevent the model from converging to the identity transform, as shown by the learned weights and magnitudes depicted at the bottom of Figure 4. We see indeed that the



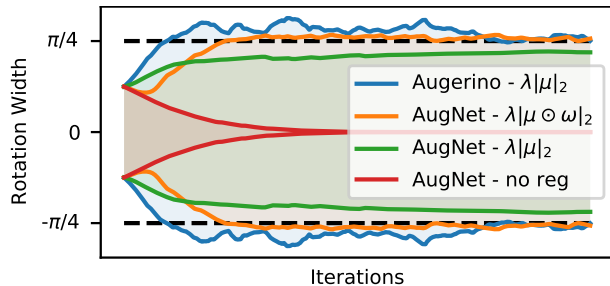


Figure 3: Learned rotation angle during training. Both Augerino Benton et al. [2020] (blue) and AugNet (orange) are able to learn the correct level of rotation invariance in the data. When the regularization is removed from AugNet (red), it converges to the identity transform (no rotation) as observed in Benton et al. [2020]. If we replace the regularizer in AugNet by Augerino’s one, AugNet misses the correct rotation angle (green).

model maximizes the weight for `translate-x` and minimizes its magnitude, while maximizing the magnitude of other transformations which have very small weights. In contrast, we can see at the top of Figure 4 that the regularizer we propose allows to both *select* the `rotate` operation and correctly tune its magnitude.

## 4.2 Application to problems beyond computer vision

In this experiment we demonstrate that AugNet is also applicable to other types of data and can learn non-linear transformations which go beyond the scope of Augerino. For this, we create a dataset consisting of four classes corresponding to 4 generating frequencies:  $\omega = 2, 4, 6$  and  $8$  Hz. For each of these frequencies, 10 seconds long sinusoidal waves of unit amplitude are created with frequencies sampled uniformly between  $\omega \pm 0.5$  Hz. Moreover, the phase of these waves are sampled uniformly and they are corrupted with additive Gaussian white noise with a standard-deviation of 0.5 (cf. Figure B.3). We generate 400 training examples and 200 test examples. The learning task consists in predicting the correct generating frequency  $\omega$  from the noisy signals. Note that, because classes are separated by 1 Hz, the dataset presents an invariance to frequency shifts of the inputs between  $\pm 0.5$  Hz.

In order to learn this invariance, we use a single augmentation layer implementing three augmentations from the EEG literature: `frequency shift` Rommel et al. [2021], `FT surrogate` Schwabedal et al. [2019] and `Gaussian noise` Wang et al. [2018]. The trunk model used is a simple 3-layer convolutional network described in Section A.2 together with other experimental settings.

As shown in Figure 5, AugNet is once again able to learn the correct range of invariance, and select the correct transformation (cf. Figure B.1 in the appendix).

## 4.3 Insensitivity to model capacity

In this experiment we aim to demonstrate that models trained with our proposed methodology are invariant regardless of the capacity of the trunk model  $f$  used, which represents an advantage over (automatic) data augmentation. For this, we re-use the sinusoids dataset from Section 4.2 and compare three methods: a baseline model trained directly on the raw data, the same model trained with an oracle augmentation  $T$  (frequency shift with bounds of  $\pm 0.5$  Hz) and an AugNet using the baseline as trunk model. Unlike in Section 4.2, we use here a very small multi-layer perceptron with a varying number of neurons and layers, in order to be able to assess the impact of the model’s expressivity.

In addition to the generalization power of the trained models, evaluated through their accuracy over the test set, we are interested in how invariant they are to the true symmetry  $T$  encoded in the data. To gauge this property for a model  $f$  at some input  $x \in \mathcal{X}$ , we use the following metric adapted from Bouchacourt et al. [2021]:

$$\text{Inv}_T(f(x)) = \frac{b - d(f(x), f(T(x)))}{b}, \quad (4)$$

where  $d$  is the cosine distance and  $b = d(f(x_i), f(x_j))$  is a baseline distance between randomly shuffled inputs<sup>1</sup>. As applying  $T$  to the inputs of an invariant model should leave its outputs unchanged, the closer  $\text{Inv}_T(f(x))$  is to 1 for various inputs  $x$ , the more  $f$  is invariant to  $T$ .

Figure 6 reports the median invariance across the test set of the three models for different number of layers and neurons. It can be seen that data augmentation helps to increase the level of invariance of the baseline model considerably. However, the level of invariance reached for the smallest models is lower than for larger models, suggesting that the former cannot encode perfectly the invariance taught to them through data augmentation. This problem would be worse in a realistic setting where augmentations are more complex and imperfectly learned by ADA approaches rather than known *a priori*. On the contrary, results show that AugNet is capable of learning the correct augmentation from scratch and make the baseline model almost perfectly invariant to it, regardless of its expressivity. Furthermore, the plot at the bottom of Figure 6 suggests that the level of invariance of each model is tightly related to its predictive performance.

<sup>1</sup>Here  $f$  refers to the activations before the final softmax.

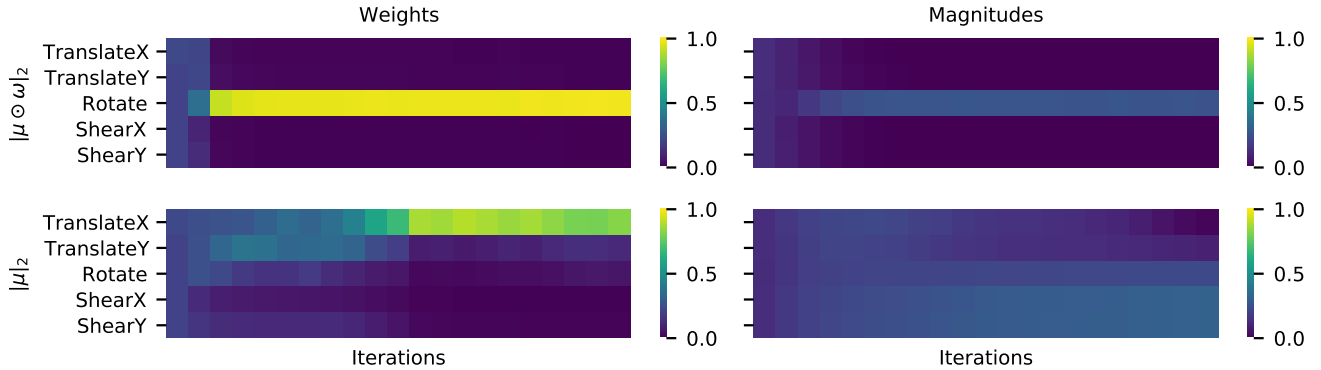


Figure 4: **Top:** With its standard regularizer, AugNet quickly learns to maximize the probability weight of rotation and adjusts the corresponding magnitude, ignoring other irrelevant transformations. **Bottom:** With Augerino’s regularizer, the model may still converge to the identity map by maximizing the probability weight of any (irrelevant) transformation and minimizing its magnitude towards 0.

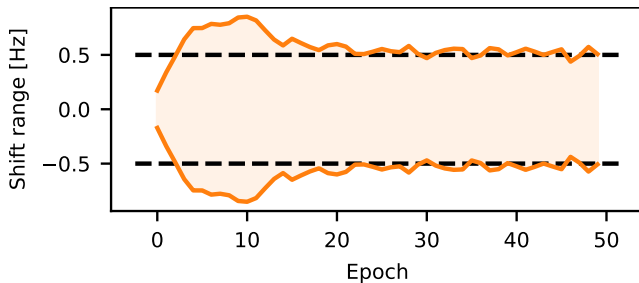


Figure 5: Learned frequency shift invariance. AugNet is able to learn nonlinear invariances from various types of data.

## 5 Experiments with real datasets

In order to illustrate the practical usefulness of the proposed approach, results of experiments carried on empirical datasets are presented in this section.

### 5.1 Image recognition

In this experiment we chose to show-case AugNet on a standard image recognition task using the CIFAR10 dataset [Krizhevsky et al. \[2009\]](#). All models considered in this experiment are trained for 200 epochs over 10 different seeds on a random 80% fraction of the official CIFAR10 training set. The remaining 20% is used as a validation set for early-stopping and choosing hyperparameters, and the official test set is used for reporting performance metrics. The trunk model used here is a pre-activated ResNet18 [He et al. \[2016b,a\]](#).

We consider three baselines in this experiment: Augerino [Benton et al. \[2020\]](#), as well as the trunk model trained alone, with and without a classical set of fixed data augmentations (horizontal flip and random crop).

A standard normalization of RGB channels using *ad-hoc* scaling factors is also applied to the model trained with fixed augmentations, and omitted for all others (*cf.* [Section A.3](#)). As for AugNet, we consider two different types of augmentation layers: *geometric layers* with the five linear augmentations detailed in [Section 4.1](#); and *non-geometric layers* with three nonlinear augmentations (contrast, brightness jitter [Howard \[2014\]](#) and sample-pairing [Inoue \[2018\]](#)). Three AugNet models were trained with an increasing number of layers: a model with a single geometric layer, a model with a non-geometric and a geometric layer, and a model with one non-geometric layer and two geometric ones. Both AugNet and Augerino were trained with a number of copies set to  $C = 1$  and tested with  $C = 4$ , as done in [Benton et al. \[2020\]](#). The reader is referred to [Section A.3](#) for further experimental settings.

[Figure 7](#) reports the test accuracy across epochs. For a given epoch, we report the test accuracy corresponding to the best validation accuracy up to that point in training (equivalent to having early-stopped the model). The performance of the baseline model with no augmentation is considerably improved by both Augerino and AugNet with one layer. This is consistent with the fact that they implement roughly the same augmentations. While adding a second layer encoding non-geometric augmentations does not seem to help, the model using 3 augmentation layers achieves top performance. Note that while the baseline using a fixed set of augmentations reaches the same final performance, it used a normalization trick that AugNet learns by itself, likely through the **brightness** transformation. Furthermore, [Results](#) show that AugNet models learn considerably faster than all three baselines, reaching test accuracy scores above 80% with 5x fewer epochs. We hypothesize that this is due to the fact that the model becomes

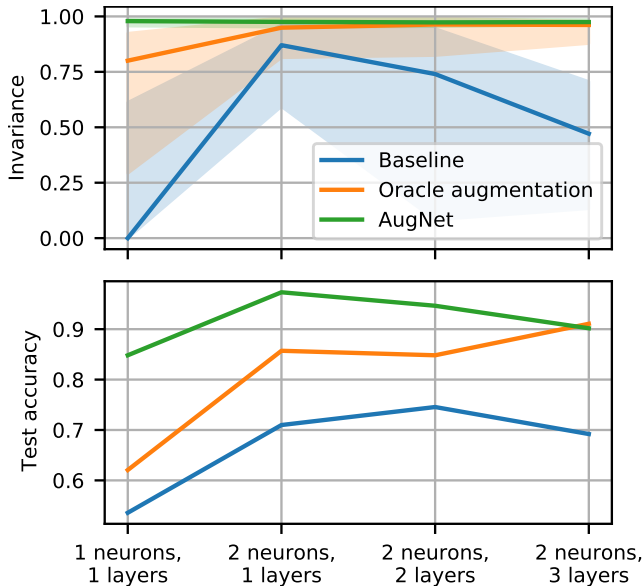


Figure 6: **Top:** Model invariance (4) to the true frequency shift in the data across different architectures. We report the median values across the test set, with a 75% confidence interval. Data augmentation helps to increase the model invariance, but is limited by its expressivity, even when data invariances are known. AugNet *learns* to be almost perfectly invariant and is insensitive to model capacity. **Bottom:** AugNet outperforms a model trained with *oracle* augmentation with 3x fewer parameters.

invariant to learned augmentations more easily at early stages of the training. Evidence for this can be found in the fact that AugNet achieves a training accuracy close to 100% after only 10 epochs, which is very early in the training compared to the other methods (*cf.* Figure B.4 in the appendix).

## 5.2 Sleep stage classification

Similarly to Section 4.2, this experiment aims to demonstrate the practical usefulness of AugNet in a realistic setting beyond affine transformations. For this, a sleep stage classification task is considered. As most commonly done [Iber et al., 2007], it consists in assigning to windows of 30s of EEG signals a label among five: Wake (W), Rapid Eye Movement (REM) and Non-REM of depth 1, 2 or 3 (N1, N2, N3). The public dataset MASS - Session 3 [O’reilly et al., 2014] is used for this purpose (more details in Section A.4). As done by Rommel et al. [2021], both the training and validation sets consist of 24 nights each, and the test set contained 12 nights. The trunk model used for this experiment is the convolutional network proposed in Chambon et al.

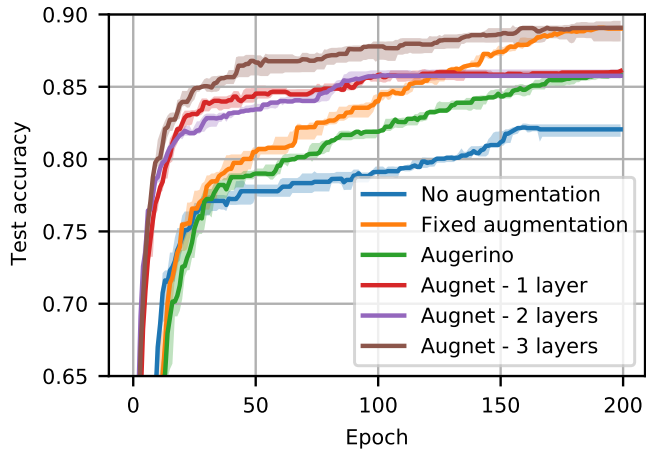


Figure 7: Median test accuracy on CIFAR10, over 10 seeds. Shades represent 1st and 3rd quartiles. AugNet reaches top performance scores faster than other methods. It learns invariances from scratch and is able to achieve a final performance equivalent to known data augmentations and preprocessings for this dataset.

[2018], whose architecture is detailed in section Section A.4 together with other experimental settings. In this experiment, we compare the proposed approach to ADA methods. For this, two discrete search methods were considered: *AutoAugment* Cubuk et al. [2019] and *Fast AutoAugment* Lim et al. [2019]. Additionally, three gradient-based methods were also tested: *Faster AutoAugment* Hataya et al. [2020], *DADA* Li et al. [2020] and *ADDA* Rommel et al. [2021]. All these methods shared the same policy architecture, consisting in 5 subpolicies made of 2 augmentation transformations (*cf.* Section A.4). As for the previous experiment, we used two types of augmentation layers to implement AugNet: two layers capable of sampling *time-frequency* transformations, and one layer made of *sensors* transformations (*cf.* Table 4).

Figure 8 presents the balanced accuracy over the test set as a function of the computation time. For ADA methods, we stopped the search every given number of steps (2 epochs or 5 samplings), used the learned policy to retrain the model from scratch (leading to a point in Figure 8) and resumed the search from where it stopped. For each run, we report the test accuracy of the best retrained model according to the validation accuracy. Also note that some methods (Fast AutoAugment and ADDA) require a pretraining of the model. Hence, the reported GPU hours for ADA methods correspond to the sum of pretraining, search and retraining time, which explains why they start with some horizontal offset. We see that, given a budget of 12 hours, AugNet is able to outperform four out of the five state-of-the-art



approaches both in speed and accuracy. It reaches a final performance comparable to the recently proposed ADDA, while requiring considerably less efforts in parameter fine tuning. AugNet only requires to set two hyperparameters: the regularization parameter  $\lambda$  which is only one-dimensional, and the number augmentation layers stacked in the network. In contrast bilevel approaches require to carefully tune jointly the learning rate and the batch size of the validation set for the outer problem. Moreover, while AugNet is trained *end-to-end* once on the training set, ADDA requires pre-training the model and a final retraining of the model with the learned augmentation policy.

ADDA approaches both in speed and final performance with *end-to-end* training, avoiding tedious bilevel setup.

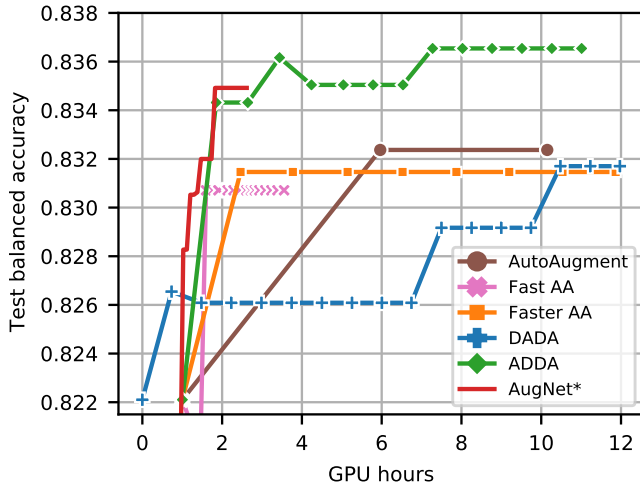


Figure 8: Median performance (over 5 folds) on the MASS dataset, as a function of the computation time. AugNet is comparable in speed and accuracy to ADDA, while being trained end-to-end.

## Conclusion

In this paper we propose a new method coined AugNet to learn data invariances from the training data, thanks to differentiable data augmentation layers embedded in a deep neural network. Our method can incorporate any type of differentiable augmentations and is applicable to a broad class of learning problems. We show that our approach can correctly select the transformation to which the data is invariant, and learn the true range of invariance, even for nonlinear operations. While (automatic) data augmentation is limited by the capacity of the model to encode symmetries, our approach leads to almost perfect invariance regardless of the model size. On computer vision tasks, this advantage allows our method to reach high generalization power with fewer epochs. Promising results are also obtained for sleep stage classification, where AugNet outperforms most

## Acknowledgements

This work was supported by the BrAIN grant (ANR-20-CHIA-0016). It was also granted access to the HPC resources of IDRIS under the allocation 2021-AD011012284 and 2021-AD011011172R1 made by GENCI.

## References

- Akiba, T., Sano, S., Yanase, T., Ohta, T., and Koyama, M. Optuna: A Next-generation Hyperparameter Optimization Framework. In *Proceedings of the 25th ACM SIGKDD International Conference on Knowledge Discovery and Data Mining*, 2019.
- Bengio, Y., Léonard, N., and Courville, A. C. Estimating or Propagating Gradients Through Stochastic Neurons for Conditional Computation. *CoRR*, 2013.
- Benton, G., Finzi, M., Izmailov, P., and Wilson, A. G. Learning Invariances in Neural Networks. In *Advances in Neural Information Processing Systems (NeurIPS)*, 2020.
- Bouchacourt, D., Ibrahim, M., and Morcos, A. S. Grounding inductive biases in natural images: invariance stems from variations in data. In *Advances in Neural Information Processing Systems (NeurIPS)*, 2021.
- Chambon, S., Galtier, M., Arnal, P., Wainrib, G., and Gramfort, A. A deep learning architecture for temporal sleep stage classification using multivariate and multimodal time series. *IEEE Transactions on Neural Systems and Rehabilitation Engineering*, 26(4): 758–769, 2018.
- Chen, S., Dobriban, E., and Lee, J. H. A Group-Theoretic Framework for Data Augmentation. In *Advances in Neural Information Processing Systems (NeurIPS)*, 2020.
- Chen, X. and Hsieh, C.-J. Stabilizing Differentiable Architecture Search via Perturbation-based Regularization. In *International Conference on Machine Learning (ICML)*, 2020.
- Cohen, T. and Welling, M. Group equivariant convolutional networks. In *International Conference on Machine Learning (ICML)*. PMLR, 2016.
- Cubuk, E. D., Zoph, B., Mane, D., Vasudevan, V., and Le, Q. V. AutoAugment: Learning Augmentation Strategies From Data. In *IEEE/CVF Conference on Computer Vision and Pattern Recognition (CVPR)*. IEEE, 2019.
- Gramfort, A., Luessi, M., Larson, E., Engemann, D. A., Strohmeier, D., Brodbeck, C., Goj, R., Jas, M., Brooks, T., Parkkonen, L., and Hämäläinen, M. S. MEG and EEG data analysis with MNE-Python. *Frontiers in Neuroscience*, 7(267):1–13, 2013.
- Grathwohl, W., Choi, D., Wu, Y., Roeder, G., and Duvenaud, D. Backpropagation through the Void: Optimizing control variates for black-box gradient estimation. In *International Conference on Learning Representations (ICLR)*, 2018.
- Hataya, R., Zdenek, J., Yoshizoe, K., and Nakayama, H. Faster AutoAugment: Learning Augmentation Strategies Using Backpropagation. In *Computer Vision – ECCV 2020*. Springer International Publishing, 2020.
- He, K., Zhang, X., Ren, S., and Sun, J. Deep residual learning for image recognition. In *IEEE/CVF Conference on Computer Vision and Pattern Recognition (CVPR)*, 2016a.
- He, K., Zhang, X., Ren, S., and Sun, J. Identity mappings in deep residual networks. In *Computer Vision – ECCV 2016*, 2016b.
- Ho, D., Liang, E., Stoica, I., Abbeel, P., and Chen, X. Population Based Augmentation: Efficient Learning of Augmentation Policy Schedules. In *International Conference on Machine Learning (ICML)*, 2019.
- Howard, A. G. Some improvements on deep convolutional neural network based image classification. *CoRR*, abs/1312.5402, 2014.
- Iber, C., Ancoli-Israel, S., Chesson, A., and Quan, S. F. The AASM Manual for the Scoring of Sleep and Associated Events: Rules, Terminology and Technical Specification, 2007.
- Inoue, H. Data augmentation by pairing samples for images classification. In *IEEE/CVF Conference on Computer Vision and Pattern Recognition (CVPR)*, 2018.
- Kingma, D. P. and Ba, J. Adam: A Method for Stochastic Optimization. In *International Conference on Learning Representations (ICLR)*, 2015.
- Krizhevsky, A., Hinton, G., et al. Learning multiple layers of features from tiny images. 2009.
- Krizhevsky, A., Sutskever, I., and Hinton, G. E. ImageNet classification with deep convolutional neural networks. In *Advances in neural information processing systems (NeurIPS)*, 2012.

- LeCun, Y., Boser, B., Denker, J. S., Henderson, D., Howard, R. E., Hubbard, W., and Jackel, L. D. Back-propagation applied to handwritten zip code recognition. *Neural Computation*, 1:541–551, 1989.
- Li, Y., Hu, G., Wang, Y., Hospedales, T., Robertson, N. M., and Yang, Y. DADA: Differentiable Automatic Data Augmentation. In *ECCV*, 2020.
- Lim, S., Kim, I., Kim, T., Kim, C., and Kim, S. Fast AutoAugment. In *Advances in Neural Information Processing Systems (NeurIPS)*, 2019.
- Liu, H., Simonyan, K., and Yang, Y. DARTS: Differentiable Architecture Search. In *International Conference on Learning Representations (ICLR)*, 2019.
- O’reilly, C., Gosselin, N., Carrier, J., and Nielsen, T. Montreal archive of sleep studies: an open-access resource for instrument benchmarking and exploratory research. *Journal of sleep research*, 23(6):628–635, 2014.
- Phan, H., Chen, O. Y., Tran, M. C., Koch, P., Mertins, A., and De Vos, M. Xsleepnet: Multi-view sequential model for automatic sleep staging. *IEEE Transactions on Pattern Analysis and Machine Intelligence*, 2021.
- Riba, E., Mishkin, D., D. Ponsa, E. R., and Bradski, G. Kornia: an Open Source Differentiable Computer Vision Library for PyTorch. In *Winter Conference on Applications of Computer Vision*, 2020.
- Rommel, C., Moreau, T., Paillard, J., and Gramfort, A. CADDA: Class-wise Automatic Differentiable Data Augmentation for EEG Signals. *arXiv preprint arXiv:2106.13695*, 2021.
- Schirrmester, R. T., Springenberg, J. T., Fiederer, L. D. J., Glasstetter, M., Eggenberger, K., Tangermann, M., Hutter, F., Burgard, W., and Ball, T. Deep learning with convolutional neural networks for EEG decoding and visualization. *Human Brain Mapping*, 2017.
- Schulman, J., Heess, N., Weber, T., and Abbeel, P. Gradient Estimation Using Stochastic Computation Graphs. In *Advances in Neural Information Processing Systems (NeurIPS)*, 2015.
- Schwabedal, J. T. C., Snyder, J. C., Cakmak, A., Nemati, S., and Clifford, G. D. Addressing Class Imbalance in Classification Problems of Noisy Signals by using Fourier Transform Surrogates. *arXiv:1806.08675*, 2019.
- van der Wilk, M., Bauer, M., John, S. T., and Hensman, J. Learning Invariances using the Marginal Likelihood. In *Advances in Neural Information Processing Systems (NeurIPS)*, 2018.
- Wang, F., Zhong, S.-h., Peng, J., Jiang, J., and Liu, Y. Data Augmentation for EEG-Based Emotion Recognition with Deep Convolutional Neural Networks. In *MultiMedia Modeling*, volume 10705, pp. 82–93. Springer International Publishing, 2018. Series Title: Lecture Notes in Computer Science.
- Zaheer, M., Kottur, S., Ravanbakhsh, S., Poczos, B., Salakhutdinov, R. R., and Smola, A. J. Deep sets. In *Advances in Neural Information Processing Systems (NeurIPS)*, 2017.
- Zela, A., Elsken, T., Saikia, T., Marrakchi, Y., Brox, T., and Hutter, F. Understanding and Robustifying Differentiable Architecture Search. In *International Conference on Learning Representations (ICLR)*, 2019.
- Zhang, M., Su, S. W., Pan, S., Chang, X., Abbasnejad, E. M., and Haffari, R. iDARTS: Differentiable Architecture Search with Stochastic Implicit Gradients. In *International Conference on Machine Learning (ICML)*, 2021.
- Zhou, A., Knowles, T., and Finn, C. Meta-Learning Symmetries by Reparameterization. In *International Conference on Learning Representations (ICLR)*, 2021.

## A Experimental settings

In all experiments, a grid-search was used to find the value of the regularization parameter  $\lambda$  from (3). In most cases, the grid of values used was 0.01, 0.1, 0.5 and 0.8. For sleep stage classification experiments, stronger values were explored: 1, 5, 10, 50.

### A.1 Mario-Iggy experiment – Section 4.1

The data was generated as described in Figure A.1 and Section 4.1. We used 10000 training examples and 5000 training examples, and sampled batches of 128 images, as in Benton et al. [2020]. The trunk model used for both Augerino and Augnet are described in Table 1. The official code from Benton et al. [2020] was used for this experiment. As in the latter, all models were trained for 20 epochs using Adam Kingma & Ba [2015], with  $\beta_1 = 0.9$  and  $\beta_2 = 0.999$ . The learning rate for Augerino was set to  $10^{-2}$  and weight decay was set to 0. The regularization parameter was set to  $\lambda = 0.05$  (medium according to Benton et al. [2020]). For AugNet, we used a learning rate of  $5 \times 10^{-4}$  and a regularization parameter of 0.5, together with weight decay of 1. Augmentations were all initialized with magnitudes equivalent to  $\pi/8$  for AugNet and Augerino. Augmentations were also initialized with uniform weights for AugNet.

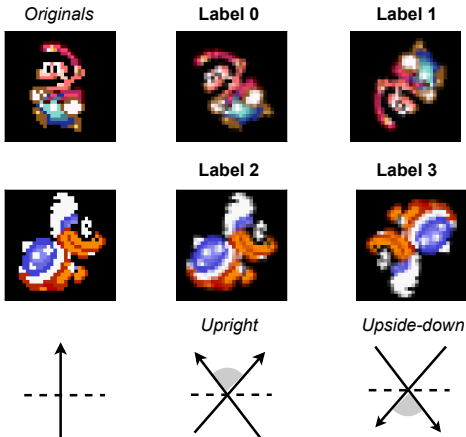


Figure A.1: Illustration of the data generation process for the Mario-Iggy experiment.

### A.2 Sinusoids experiment – Section 4.2

The data was generated as described in Figure B.3 and Section 4.2. We used 400 training examples and 200 training examples, and sampled batches of 32 waves. The trunk model used for Augnet is described in Table 2. All models were trained for 50 epochs using

|   | layer   | # filters | size | stride | batch norm |
|---|---------|-----------|------|--------|------------|
| 1 | Conv2D  | 32        | 3    | 1      | yes        |
|   | ReLU    |           |      |        |            |
| 2 | Conv2D  | 64        | 3    | 1      | yes        |
|   | ReLU    |           |      |        |            |
|   | MaxPool |           | 2    |        |            |
| 3 | Conv2D  | 128       | 3    | 1      | yes        |
|   | ReLU    |           |      |        |            |
|   | MaxPool |           | 2    |        |            |
| 4 | Conv2D  | 256       | 3    | 1      | yes        |
|   | ReLU    |           |      |        |            |
|   | MaxPool |           | 2    |        |            |
| 5 | MaxPool |           | 4    | 1      |            |
|   | FC      |           |      |        |            |
|   | Softmax |           |      |        |            |

Table 1: Convolutional neural network architecture used in experiments of Section 4.1.

Adam Kingma & Ba [2015]. We used a learning rate of  $10^{-2}$  and a regularization parameter of 0.2, together with weight decay of  $10^{-4}$ . Augmentations were all initialized with magnitudes  $\mu = 0$  and uniform weights. For the experiment of Section 4.3, we set the number of copies to  $C = 10$  at inference, while it was set to  $C = 4$  for all other experiments. Moreover,  $\lambda$  was set to 0.8 and initial magnitudes set to 0.05 in Section 4.3.

|   | layer      | # filters | size | stride | batch norm |
|---|------------|-----------|------|--------|------------|
| 1 | Conv2D     | 2         | 3    | 1      | yes        |
|   | ReLU       |           |      |        |            |
| 2 | Conv2D     | 2         | 3    | 1      | yes        |
|   | ReLU       |           |      |        |            |
|   | MaxPool    |           | 2    |        |            |
| 3 | GlobalPool |           |      |        |            |
|   | FC         |           |      |        |            |
|   | Softmax    |           |      |        |            |

Table 2: Convolutional neural network architecture used in experiments of Section 4.2

### A.3 CIFAR10 experiment – Section 5.1

Following Benton et al. [2020], we used batches of 128 images. The official code from Benton et al. [2020] was used for this experiment. As in the latter, all models were trained for 200 epochs using Adam Kingma & Ba [2015]. Also, as described in Benton et al. [2020], we used a cosine annealing scheduler with epoch  $T = 200$  epochs. For the baseline using fixed augmentations, the following normalization was used as a preprocessing of the whole dataset: centering by (0.485, 0.456, 0.406) and scaling by (0.229, 0.224, 0.225). For Augerino and the

other two baselines, the learning rate was set to  $10^{-2}$  and weight decay was set to 0. for the augmentation and  $10^{-4}$  for the trunk model. The regularization parameter was set to  $\lambda = 0.01$  for Augerino. For all three AugNet models, we used a learning rate of  $5 \times 10^{-4}$ , together with weight decay of 1 for the augmentation and  $10^{-4}$  for the trunk model. The regularization parameter was set to 0.1 for models with one a two layers, and to 0.5 for the model with three layers. Augmentations were all initialized with magnitudes equivalent to 0.5 and uniform weights for AugNet. In this experiments, differentiable augmentations were implemented using the KORNIA package [Riba et al. \[2020\]](#), as well as the official code of Faster AutoAugment [Hataya et al. \[2020\]](#).

It is worth noting that the official code used a smaller trunk model with 13 layers, which we replaced by a Pre-activate ResNet18 which significantly improved performances. It also did not implement any cosine annealing despite what was reported in [Benton et al. \[2020\]](#). We were hence not able to reproduce their results exactly.

#### A.4 MASS experiment – Section 5.2

**Dataset** The public dataset MASS - Session 3 [\[O’reilly et al., 2014\]](#) was used for this purpose (more details in [Section A.4](#)). It corresponds to 62 nights, each one coming from a different subject. Out of the 20 available EEG channels, referenced with respect to the A2 electrode, we used 6 (C3, C4, F3, F4, O1, O2). As done by [Rommel et al. \[2021\]](#), both the training and validation sets consisted of 24 nights each, and the test set contained 12 nights.

**Architecture** For all EEG experiments, learning was carried using the convolutional network proposed in [Chambon et al. \[2018\]](#), whose architecture is described on [Table 3](#). The initial number of channels  $C$  was set to 8. The first layers (1-4) implements a spatial filter, computing virtual channels through a linear combination of the original input channels. Then, layers 5 to 9 correspond to a standard convolutional feature extractor and last layers implement a simple classifier.

**Training hyperparameters** The optimizer used for all models was Adam with a learning rate of  $10^{-3}$ ,  $\beta_1 = 0.$  and  $\beta_2 = 0.999$ . At most 300 epochs were used for training, with a batch size of 16. Early stopping was implemented with a patience of 30 epochs. For ADDA, the policy learning rate was set to  $5 \times 10^4$  based on a grid-search carried using the validation set. For AugNet, the regularization parameter was set to  $\lambda = 10$ . Balanced accuracy was used as performance metric using the inverse of original class frequencies as balancing weights. The MNE-PYTHON [\[Gramfort et al.,](#)

[2013\]](#) and BRAINDECODE software [\[Schirrmester et al., 2017\]](#) were used to preprocess and learn on the EEG data. Training was carried on single Tesla V100 GPUs.

**Augmentations considered** The 13 operations considered are listed in [Table 4](#). A detailed explanation of their implementation can be found in the appendix of [Rommel et al. \[2021\]](#). While all this augmentations were used by gradient-free algorithms, **bandstop filter** was not included in the differentiable strategies (Faster AA, DADA, ADDA, AugNet) because we did not implement a differentiable relaxation of it. All augmentations used came from the BRAINDECODE package [\[Schirrmester et al., 2017\]](#). AutoAugment was implemented replacing the PPO searcher with a TPE searcher (as in Fast AutoAugment). The OPTUNA package was used for that matter [Akiba et al. \[2019\]](#).

## B Complementary results

### B.1 Sinusoids experiment – Section 4.2

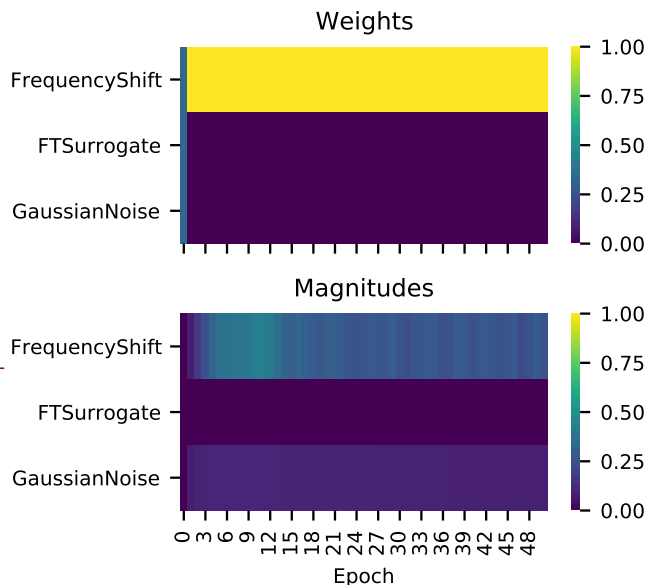


Figure B.1: Evolution of learned weights and magnitudes in the sinusoids experiment [Section 4.2](#). AugNet quickly learns to maximize the frequency shift invariance and drop the others.

### B.2 CIFAR10 experiment – Section 5.1



|    | layer         | # filters | # params               | size    | stride  | output dim.          | activation |
|----|---------------|-----------|------------------------|---------|---------|----------------------|------------|
| 1  | Input         |           |                        |         |         | (C, T)               |            |
| 2  | Reshape       |           |                        |         |         | (C, T, 1)            |            |
| 3  | Conv2D        | C         | C * C                  | (C, 1)  | (1, 1)  | (1, T, C)            | Linear     |
| 4  | Permute       |           |                        |         |         | (C, T, 1)            |            |
| 5  | Conv2D        | 8         | 8 * 64 + 8             | (1, 64) | (1, 1)  | (C, T, 8)            | Relu       |
| 6  | Maxpool2D     |           |                        | (1, 16) | (1, 16) | (C, T // 16, 8)      |            |
| 7  | Conv2D        | 8         | 8 * 8 * 64 + 8         | (1, 64) | (1, 1)  | (C, T // 16, 8)      | Relu       |
| 8  | Maxpool2D     |           |                        | (1, 16) | (1, 16) | (C, T // 256, 8)     |            |
| 9  | Flatten       |           |                        |         |         | (C * (T // 256) * 8) |            |
| 10 | Dropout (50%) |           |                        |         |         | (C * (T // 256) * 8) |            |
| 11 | Dense         |           | 5 * (C * T // 256 * 8) |         |         | 5                    | Softmax    |

Table 3: Detailed architecture from [Chambon et al. \[2018\]](#), where  $C$  is the number of EEG channels and  $T$  the time series length.

| type      | transformation    | range         |
|-----------|-------------------|---------------|
| Time      | time reverse      |               |
|           | time masking      | 0-200 samples |
|           | Gaussian noise    | 0-0.2 std     |
| Frequency | FT-surrogate      | 0- $2\pi$     |
|           | frequency shift   | 0-5 Hz        |
|           | bandstop filter   | 0-2 Hz        |
| Sensors   | sign flip         |               |
|           | channels symmetry |               |
|           | channels shuffle  | 0-1           |
|           | channels dropout  | 0-1           |
|           | rotations x-y-z   | 0-30 degrees  |

Table 4: Augmentations considered in experiment 5.2. The range column corresponds to the values to which are mapped the magnitudes  $\mu = 0$  and  $\mu = 1$ .

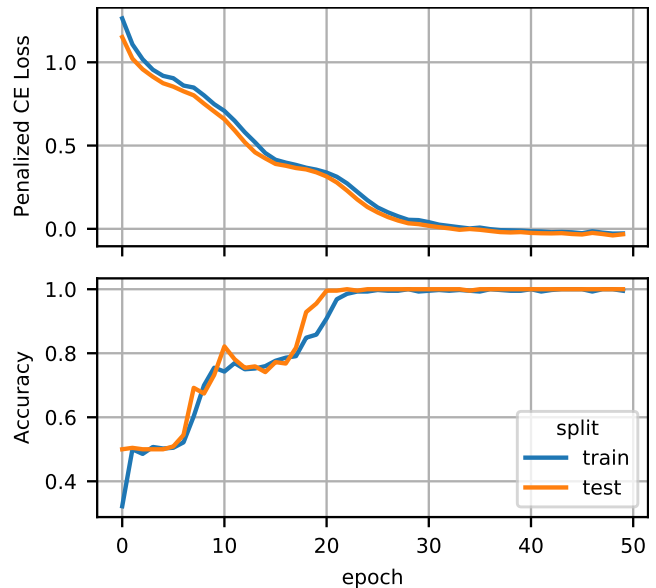


Figure B.2: Loss and accuracy during AugNet training in the sinusoids experiment [Section 4.2](#)

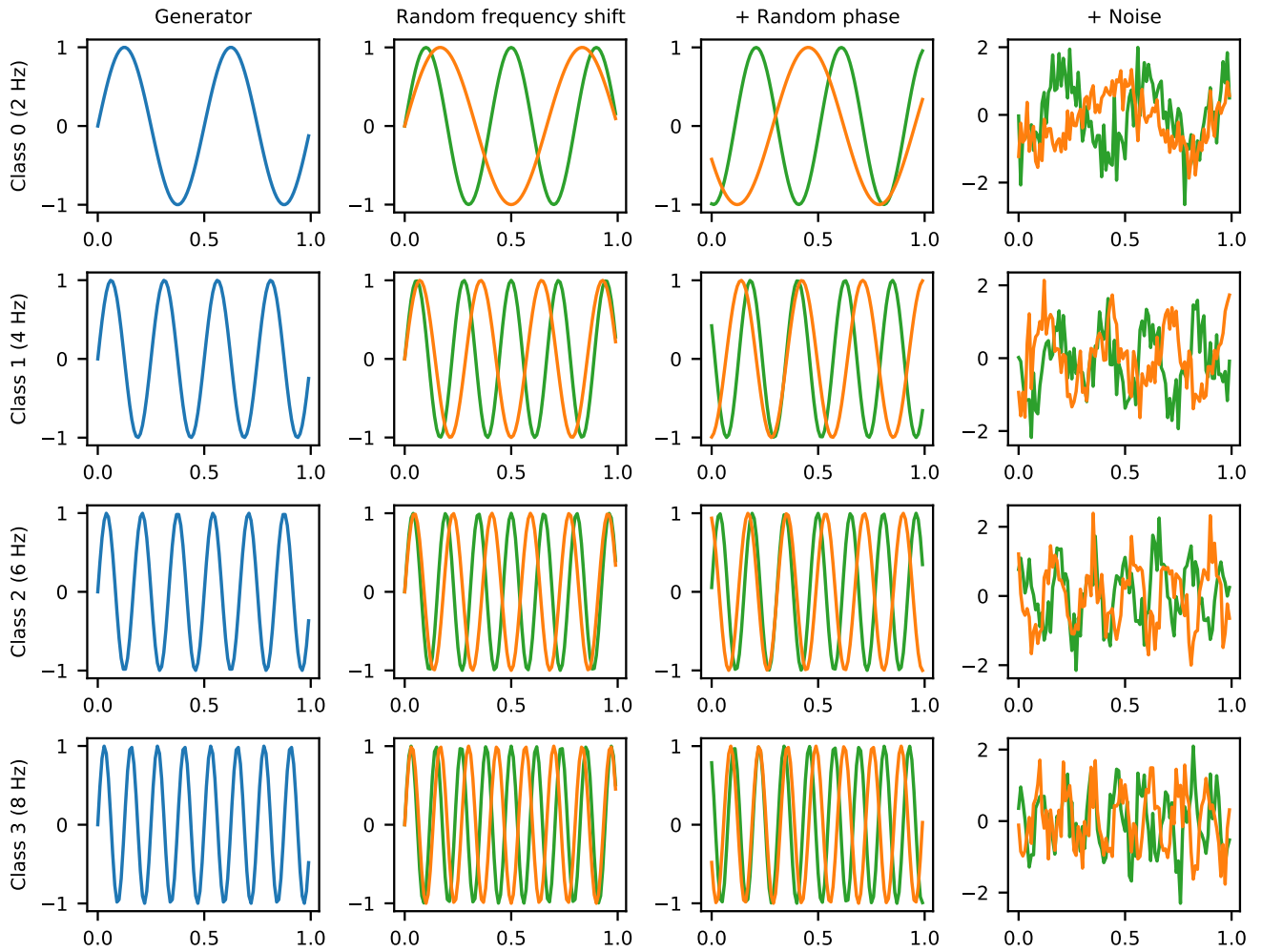


Figure B.3: Illustration (cropped to 1 second) of waves composing each class of the simulated dataset used in the sinusoids and model capacity experiments.

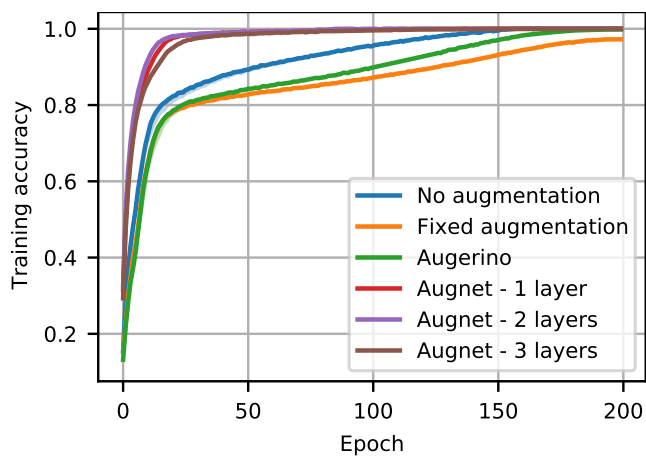


Figure B.4: Training accuracy across epochs in the CIFAR10 experiment 5.1. AugNet reaches accuracies near 100% after a few epochs, way earlier than other models. We hypothesize this is due to its near perfect invariance to relevant transformations which are quickly learned.